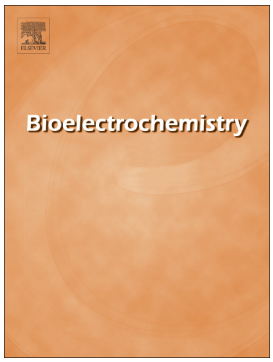

Electrochemical xanthine detection by enzymatic method based on Ag doped ZnO nanoparticles by using polypyrrole

Buket Yalcin Sahyar, Merve Kaplan, Mehmet Ozsoz, Erdal Celik, Semih Otles

PII: S1567-5394(19)30309-3
DOI: https://doi.org/10.1016/j.bioelechem.2019.107327
Article Number: 107327
Reference: BIOJEC 107327

To appear in: *Bioelectrochemistry*

Received date: 8 May 2019
Revised date: 1 July 2019
Accepted date: 2 July 2019

Please cite this article as: B.Y. Sahyar, M. Kaplan, M. Ozsoz, et al., Electrochemical xanthine detection by enzymatic method based on Ag doped ZnO nanoparticles by using polypyrrole, Bioelectrochemistry, https://doi.org/10.1016/j.bioelechem.2019.107327

Electrochemical Xanthine Detection by Enzymatic Method Based on Ag doped ZnO Nanoparticles by Using Polypyrrole

Buket Yalcin Sahyar[a,*] buket.yalcin.35@gmail.com, Merve Kaplan[b] meervekaplan@gmail.com, Mehmet Ozsoz[c] mehmet.ozsoz@neu.edu.tr, Erdal Celik[d] erdal.celik@deu.edu.tr, Semih Otles[a] semih.otles@ege.edu.tr

[a]Ege University, Engineering Faculty, Food Engineering Department, 35100 Bornova, Izmir, Turkey
[b]Independent researcher, Izmir, Turkey
[c]Faculty of Engineering, Near East University, Lefkosa TRNC Via Mersin 10 – Turkey
[d]Dokuz Eylul University Faculty of Engineering Dept. of Metallurgical and Materials Engineering, Tinaztepe Campus, 35397 Buca, Izmir, Turkey
[*]Corresponding author.

Abstract

A sensitive electrochemical detection of xanthine (X), which is an early biomarker of fish meat spoilage, was achieved by a novel biosensor developed via three main steps. The first step is the electropolymerization of a conducting polymer (pyrrole) onto the pencil graphite electrode (PGE). The second step is the entrapment of silver-doped zinc oxide nanoparticles (nano Ag–ZnO) onto PGE, which has already been doped with polypyrrole (PPy). The third step is the immobilization of the enzyme (xanthine oxidase) onto the modified electrode (nano Ag–ZnO/PPy/PGE) surface. The biosensor was characterized by scanning electron microscopy (SEM). The addition of Ag-doped ZnO nanoparticles into the conducting polymer structure played an important role in the performance of the biosensor by increasing the porous structure of the conducting polymer surface. The electrochemical behaviour of the biosensor was studied by electrochemical impedance spectroscopy (EIS) and chronoamperometry (CA). This enzyme biosensor showed the maximum response at pH 7.40 when +0.7 V was applied to reach 95% of steady-state current at ~3.2 s. The designed biosensor showed high selectivity with a sensitivity of 0.03 µA/mM and a low detection limit of 0.07 µM.

Keywords: Amperometry, Biosensor; Fish meat; Nanoparticle; Xanthine.

Abbreviations

PGE	pencil graphite electrode
X	$C_5N_4O_2H_4$ xanthine
ATP	adenosine triphosphate
ZnO	zinc oxide
Ag	silver
XOD	xanthine oxidase
PPy	polypryrrole
HPLC-DAD	high pressure liquid chromatography with diode-array detection
s	second
µA	microampere
RSD	relative standard deviation
IMP	inosine monophosphate
nano ZnO	nanoparticle based zinc oxide
NanoAgZnO	nanoparticle based silver doped zinc oxide
LOD	limit of detection
Py	pyrrole
PBS	phosphate buffer solution

ABS	acetate buffer solution
$HClO_4$	XRD X-ray diffraction
XPS	X-ray photoelectron spectrometer
SEM	scanning electron microscopy
U	enzyme unit
R_{ct}	charge transfer resistance
HX	hypoxanthine
UA	uric acid
Co_3O_4	cobalt oxide
CH	chitosan
GR	graphene
MWCNTs	multiwalled carbon nanotubes
GCE	glassy carbon electrode
BQ	1,4-benzoquinone
NPs	nanoparticles
FTO	fluorine doped tin oxide, mAU, the intensity of absorbance (in units of mAU or milli-Absorbance Units)
transmittance	T
intensity	I

1. Introduction

Fish meat is a fundamental source of protein and other nutrients for people but it is very delicate and easily spoiled. Spoilage is the degradation of fish meat by the change in physical properties. It involves complex reactions that are triggered by the death of the fish (post mortem period). Fish meat spoilage generally starts with microbial contamination. Further, autocatalytic reactions occur by endogenous enzymes, which are present in the intestine and muscle tissues. The post mortem period of fish meat is associated with the decomposition of nucleotides—during these reactions, the rapid degradation of ATP produces a significant increase in the concentration of inosine, which is subsequently transformed to hypoxanthine and xanthine by bacterial metabolism; this degradation sequence has been studied since the early 1950s, and it is known to correlate well with the degree of spoilage. All these biochemical reactions change the texture, flavor, and color of fish meat. In the early stage, ATP degradation gives a desirable flavor to fish meat with the formation of IMP (inosine monophosphate). When IMP starts to turn into xanthine, the taste of fish meat starts to turn into undesirable flavors. That is why xanthine was selected as a biomarker in this study, since it represents the early stage of fish meat spoilage. Xanthine ($C_5H_4N_4O_2$) is generally found in body tissues and fluids and is produced by guanine deaminase from guanine and/or xanthine oxidase from hypoxanthine. A variety of stimulants are derived from xanthine, including caffeine and theobromine [1–7]. Xanthine concentration can be consequently measured by xanthine biosensors, which thus provide information on fish and meat spoilage. The most commonly used methods for monitoring xanthine are high-pressure liquid chromatography (HPLC), fluorometric mass spectrometry fragmentography, gas chromatography, and ELISA (enzyme-linked immunosorbent assay) [5,8–17]. However, these methods included drawbacks such as the requirement of a long sample preparation time, an expensive apparatus which needs to be operated by a skilled person, and a lack of high specificity and sensitivity. These drawbacks can be overcome using devices such as biosensors [1,5,6,14,18–21]. The electrochemical reaction of xanthine biosensors is based on the reaction below [14,22]:

$$\text{Xanthine} + O_2 + H_2O \xrightarrow{\text{XOD}} \text{Uric Acid} + H_2O_2 \quad (1)$$

$$H_2O_2 \rightarrow 2H^+ + O_2 + 2e^- \quad (2)$$

$$2e^- \rightarrow \text{electrode (current)} \quad (3)$$

Xanthine oxidase has been widely used for biosensor designing for the fast quantitative analysis of xanthine in real samples [14,22], by immobilizing it on various conducting polymers, such as Nafion membrane [9], polypyrrole (PPy) film [23,24], and polyvinyl chloride (PVC) membrane [12]. However, these conducting polymers have significant drawbacks such as slow electron transfer, poor stability, reusability, non-conducting and non-elastic properties, fragility, and poor absorption ability [6]. Therefore, the introduction of a system modified by an electron transfer mediator is necessary to achieve the highly desirable lower detection limit and faster electron transfer [14]. The unique electronic properties of nanomaterials have been widely exploited in electrochemistry as a means of promoting the electron transfer reaction for a wide range of biosensor applications [25]. To overcome these

requirements, Ag-doped ZnO nanoparticles were used. The specific influence of a doped nanoparticle biosensor involves increasing the surface area to obtain a reasonable response with minimum material usage while providing a lower detection limit and faster electron transfer. The benefit of doping Ag ions onto ZnO from the literature is that Ag is the most suitable p-type doping agent for ZnO (because of its larger ionic size, high solubility, and minimum orbital energy) [26–29].

In this study, a novel xanthine-based biosensor (nano Ag–ZnO/PPy/pencil graphite electrode (PGE)) was prepared successfully to detect and determine the xanthine content of the fish meat sample. The detection of xanthine (X) was conducted amperometrically at 0.7 V. The limit of detection (LOD) was 0.07 µM. Selectivity, checked with hypoxanthine (HX) and uric acid (UA), proved to be very high. This assay can be easily applied for the detection of xanthine in real fish meat samples.

2. Experimental

The experimental procedure followed throughout this study is summarized in Schematic 1 and can be divided into four steps as follows: (1) the electropolymerization of pyrrole onto PGE, (2) the entrapment of nano ZnO (A) and nano Ag–ZnO (B) onto PGE doped with polypyrrole, (3) the immobilization of xanthine oxidase (XOD) enzymes, and (4) the electrochemical measurement.

2.1.Materials

2.1.1. Reagents and solutions

Xanthine oxidase (XOD, 99.9%), xanthine (X, $C_5N_4O_2H_4$, 99%), pyrrole (Py, 99.5%), hydrochloric acid (HCl, 37%), phosphate buffer solution (PBS, 99.9%), 0.5 M acetate buffer solution (ABS), ethanol (99%), and perchloric acid ($HClO_4$) were obtained from Sigma. Sodium hydroxide (NaOH, 96%) and sodium perchlorate ($NaClO_4$) were obtained from BDH. Hydrogen peroxide (H_2O_2, 35%) was obtained from Merck. Potassium chloride (KCl, powder, 25%) and potassium ferricyanide ($K_3Fe[(CN)_6]$) were obtained from Kimetsan.

2.1.2. Apparatus

A three-electrode system was used in electrochemical studies, including pencil graphite lead (Tombow 2B, 0.5 mm, Japan) as the working electrode, a platinum wire as the auxiliary electrode, and Ag/AgCl (with 3mol/L KCl electrolyte) as the reference electrode. The system was connected to an Autolab PGSTAT204 compact and modular potentiostat/galvanostat. The measurements were achieved by NOVA 1.1 (Metrohm Autolab, Turkey) and Origin Pro 8 software. HPLC-DAD (Agilent 1200, ABD), X-ray diffraction (XRD, Thermo Fisher, Arl-Alpha, USA), Fourier transform infrared spectrometry (FTIR, Perkin Elmer, USA), X-ray

photoelectron spectrometry (XPS, Thermo Fischer, Al-Kα, USA), and scanning electron microscopy (SEM, JEOL, JSM 6060, Tokyo, Japan) were used. Minitab Statistical Software (Minitab17) was used for statistical analysis.

2.2. Nanoparticle preparation

Doped ZnO nanoparticles are good supplementary particles for polymeric materials (PPy). These polymeric materials are widely used for the construction of biosensors, using a precursor solution (including polymeric materials, doped nanoparticles, and solvents). However, precursor solutions must be transparent, well dispersed, homogeneous, and uniform. Additionally, the size of the nanopowder (doped nanoparticles) is a very significant parameter to prepare a feasible biosensor. On the other hand, decreasing the size of nanopowders directly increases the usable surface area of the biosensor to achieve efficient detection. Hence, after numerous studies on different doping agents, Ag ions were selected. Undoped ZnO nanoparticles were also prepared to make a comparison. The feasible p-type doping characteristic of Ag ions for ZnO nanoparticles as well as for the homogeneous, well dispersed, and uniform polymeric matrix structure of Ag-doped ZnO nanoparticles for the formation of biosensors were the main benefits of Ag ions for use as doping agents in this study. The production steps for Ag-doped ZnO nanoparticles can be summarized as follows. Firstly, precursor solution was prepared by a bulk material mixture of $Zn(NO_3)_2$ and $AgNO_3$ (w/w %) for the preparation of ZnO and Ag-doped ZnO nanoparticles. The precursor was dissolved in methanol (1:1 weight of bulk material/volume of solvent). Glacial acetic acid was used as a chelating agent. After these production steps, characterization (XRD, FTIR, XPS, and SEM) analyses were carried out to control the nanoparticles (ZnO and nano Ag–ZnO). A homogeneous solution was obtained by magnetic stirring for 15 min at room temperature in a taped bottle. To chelate the gelation reactions, 0.5 mL glacial acetic acid was added to the sol–gel solution. This solution was kept at 70 °C for 30 min and 150 °C for ~30–60 min to obtain the bulk material, and resulting gel was dried at 70 °C overnight in an oven to form a precursor for ZnO nanoparticles. Then, the obtained xerogel was dried at 300 °C for 15 min and 500 °C for 15 min. Finally, the dry gel powder was eventually calcined at 600 °C for 3 h in air to obtain sol–gel-assisted crystalline nanopowders. After the calcination step, impurities and excesses of carbon monoxide, carbon dioxide, and water were removed. Then, the high-purity nanopowders obtained and were milled to yield suitable nanosized materials (~80 nm) [30,31].

2.3.Design of biosensor

The biosensor was designed in three steps: Ppy formation on the PGE, entrapment of nanoparticles onto the Ppy, and enzyme immobilization.

2.3.1. Pretreatment of Electrodes

The most crucial step in the biosensor design is the electropolymerization of pyrrole to achieve a uniform surface coverage of PPy. Pretreatment of bare PGE electrode is necessary before the electropolymerization step to remove any impurities from the surface. To do this, +1.40 V (vs. Ag/AgCl) was applied for 60 s in 0.50 M acetate buffer solution (ABS, pH 4.8). The solution was stirred during application [32].

2.3.2. Electropolymerization of pyrrole

The electropolymerization of Py was performed using cyclic voltammetry with six cycles, a 30 mv/s scan rate, and scanning between 0 V and +0.80 V in a solution consisting of 0.15 M Py and 100 mM $NaClO_4$ dissolved in PBS (0.05 M, pH: 7.4, 20 mM NaCl) [32].

2.3.3. Entrapment of nanoparticles (ZnO and Ag-ZnO)

The entrapment of the nanoparticles was performed by cyclic voltammetry with six cycles, a 30 mv/s scan rate, and scanning between 0 V and +0.80 V in a solution consisting of 0.15 M ZnO or Ag–ZnO, as well as 100 mM $NaClO_4$ dissolved in PBS (0.05 M, pH 7.4, 20 mM NaCl).

2.3.4. Immobilization of enzyme (XOD)

XOD (0.15 U-µmol/min) was immobilized onto the modified electrode surface using electrochemical deposition under an open circuit potential for 15 min. Then modified electrode was washed with 50 mM PBS (pH 7.4) in order to remove any trace of undoped XOD.

2.3.5. Amperometric Measurements

For amperometric measurements, a working potential (+0.70 V) was applied and transient currents were allowed to decay to steady-state values before the injections of the substrates. Subsequently, current-time recordings were obtained under batch conditions with stirring at 400 rpm.

2.3.6. Electrochemical Measurements

The EIS measurements were carried out in the mixture of $[Fe(CN)_6]^{3-/4-}$ (2.5 mM, 1:1) redox solution prepared in 0.1 M KCl at a frequency range of 10^{-1} Hz to 10^{5} Hz, which was divided into 60 logarithmically equidistant points. The DC voltage (+0.23 V) versus Ag/AgCl and sinusoidal AC signal (10 mV) was applied throughout all EIS measurements. The diameter of the semicircle of the Nyquist plot corresponds to the charge transfer resistance Rct of the

electrode surface and was calculated by the electrochemical circle fit in AUTOLAB 302 Nova 1.10.3 software [33].

2.4.Characterization of nanoparticles and sensors

The characterization of nanoparticles and sensor were achieved via XRD, FTIR, XPS and SEM.

2.5.Chromatographic analysis of fish meat

2.5.1. Extraction method of fish meat

Fish meat tissues (~5 g) were cut into smaller pieces and then homogenized with cold perchloric acid (0.6 M; 15 mL/4 min/4 °C) using a stomacher (IUL Instrument, Barcelona, Spain). After homogenization, centrifugation was performed (10 g/20 min/4 °C) and the supernatant liquid was filtered. Then, neutralization was conducted for 30 min by adding solid potassium carbonate at 4 °C until the pH value reached 6.5–7.0. Finally, the extract was stored at 4 °C. Fish meat extract was dissolved and centrifuged (5 min/4 °C) before being using for HPLC-DAD and amperometry [5].

2.5.2. HPLC analysis of fish meat

A sample of 10 μL fish meat extract or standard solution (Xanthine) was used for HPLC-DAD analysis. μ-bondapak C18 3.9 × 300 mm 10 μm (Agilent Tech, CA, USA) column was employed, which was conditioned to 30 °C during HPLC analysis, and potassium buffer solution (50 mM, pH 4.0) was used as the mobile phase. HPLC analysis was conducted using gradient elution. The gradient elution was applied for 20 min. One hundred percent mobile phase was used in the first 10 min with 0.8 mL/min flow rate. Then, 60% methanol was used in the next 10 min with the same flow rate. Xanthine was detected at a 290 nm wavelength [14].

3. Results and discussion

3.1.Nanoparticle Selection

The benefits of Ag-doped ZnO can be seen easily from the literature review. To select the most suitable doping agent, aluminum (Al), silver (Ag), copper (Cu), and stearic acid as a modification agent (Md) were used as doping agents for ZnO. The characterization with XRD, FTIR, and XPS of nano ZnO, nano Al-doped ZnO, nano Ag-doped ZnO, nano Cu-doped ZnO, and nano Md–ZnO was successfully conducted after the production of these nanoparticles. Five modified electrodes were prepared (modified electrode preparation was performed using the methods defined in Sections 2.3.1-2.3.3) using doped nanoparticles

separately (nano ZnO, nano Al–ZnO, nano Ag–ZnO, nano Cu–ZnO and nano Md–ZnO). Then amperometric measurements were conducted (using the methods defined in Section 2.3.5), and the most suitable result was obtained from Ag–ZnO thanks to the lower charge transfer resistance (Rct) values and standard deviations (Figure 1A,B).

The characterization of nano ZnO and nano Ag–ZnO (Figure 1 and Figure 2) was performed after the production of these nanoparticles via XRD, FTIR, and XPS. The produced nano-based powder structures were defined as nano ZnO and nano Ag–ZnO, according to XRD and FTIR results (Figures 2A,B). Bibliographic research proved these results and Ag occurrence was also confirmed by (Ag) 38.22° (2θ), 44.32°, and 66.5° according to the XRD results, corresponding to (111), (200) and (200) planes of silver, while 31.86°, 34.52°, 36.32°, 47.64°,56.7°, 62.98°, 68.04° and 69.18° corresponding to (100), (002), (101), (102), (110), (103), (112) and (201) planes of ZnO and (111), (200) planes of zinc oxide, which are observed and compared with the standard powder diffraction card of Joint Committee on Powder Diffraction Standards (JCPDS), zinc oxide file No. 89-1397 and silver file No. 04–0783 (Figure 2A) [34–38]. The XRD results denoted pure a wurtzite phase formation of ZnO (JCPDS (Joint Committee on Powder Diffraction Standards), card No. 89–1397) without any crystalline phase. The ZnO nanoparticle lattice and Ag-doped ZnO lattice shape could be seen. The XRD results also showed that Ag doping successfully occurred without the existence of any impurity peak (Ag element phase, Ag_2O) [31]. FTIR was used to further explore the chemical bonding between the ZnO and Ag nanoparticles. FTIR spectrum revealed the presence of a stretching vibrational bond of O–H (3422 cm^{-1}), indicating the presence of surface-adsorbed water molecules and hydroxyl groups; O=C=O (1800–2000 cm^{-1}) represents the presence of atmospheric CO_2; C–O (1450 cm^{-1}) represents stretching; C–H (3080 cm^{-1}) represents stretching of methyl groups [39–42]. XPS analysis was performed to determine the chemical bonding state of compounds and elements and the presence of elements Zn_2p_3, O_{1s}, and Ag_3d, as seen in Figure 2C. Electron transfer was supposed to occur from Zn to Ag nanoparticles, due to the high electronegativity of Ag. The chemical bond between ZnO and Ag is one reason for the silver effect in controlling defects at ZnO crystal lattice [41].

3.2.Optimization of Biosensor

The fabrication of the biosensor means the fabrication of the working electrode. The steps for the fabrication of working electrodes are: the pretreatments of the electrode, the electropolymerization of pyrrole, the entrapment of nanoparticles onto the electrode surface, and the immobilization of the enzyme onto the electrode surface. These fabrication parameters influence the electrode working capability and the efficiency of the biosensor. For this reason, we focused on optimization steps. The pyrrole concentration, number of cycles for electropolymerization, scan rate, time of enzyme immobilization, enzyme concentration, and substrate concentration are parameters which affect the optimum working mechanism of the biosensor. The diameter of the semicircle of Figures 3A–C (Supporting figure 1A-C) is equal to the electron transfer resistance, R_{ct}, which corresponds to the electron transfer limited

process. The decrease of the R_{ct} value suggested that when the conducting polymer film was prepared on the bare electrode surface, a barrier of the polymer film would increase the electron transfer efficiency and decrease the R_{ct} value. Thus it can be concluded for R_{ct}-related optimization studies that decreasing the R_{ct} value results in an increase of the electron transfer efficiency, which means the prepared electrode will better represent the sensibility, detection mechanism, and reliability of the biosensor. The determination of the optimization parameters for Figures 3A–C was done according to this definition [14]. The oxidation of polypyrrole is an important step to reach the optimum conductivity, stability, and electrochemical activity of the prepared electrode. Firstly, the pyrrole concentration was optimized by changing the concentration from 0.01 M to 0.25 M (Figure 3A) in the solution [23]. The electron transfer reactions and charge transfer resistance (R_{ct}) values were decreased dramatically to almost 18–22 Ω R_{ct} values between 0.1 and 0.2 M Py concentration, and the most stable standard deviation was seen at 0.15 M Py concentration. After reaching a 0.15 M pyrrole concentration, the bare electrode surface became saturated with polypyrrole and over-oxidation occurred. For that reason, the 0.15 M pyrrole concentration was used for electropolymerization. Secondly, to determine the optimum polymer thickness, different scan numbers (two, four, six, eight, and ten scans) were used during the pyrrole electropolymerization process and their biosensor responses to the substrate were compared by keeping the other parameters constant. As can be seen in Figure 3B, after two scans of cyclic voltammetry (CV) the R_{ct} values decreased until six scans, then started to increase. Therefore, the optimum number of cycle repetition was determined as six [6]. The polymer layer thickness is one of the important parameters needed to provide a suitable environment for the enzyme immobilization step. The optimum polymer thickness maintains a better morphology and film quality for the biosensor [43]. Also, as Dubal et al. (2012) [44] mentioned that the scan rate affects the properties of PPy, the conductivity increased due to the oxidation of Py monomers and low-density packing occurred more at high scan rates, causing the R_{ct} value to increase [44]. The optimum scan rate was determined while changing the scan rate from 20 to 200 mV/s. As can be seen in Figure 3C, the lowest R_{ct} values were observed at 30 mV/s, after which they started to increase again. So, 30 mV/s was chosen as the scan rate. In order to achieve effective results, it is important to use the proper amount of enzyme. The optimum concentration of the enzyme was determined by changing the enzyme concentration from 0.07 to 0.20 U (µmol/min). As can be observed in Supporting Figure 2A, the maximum response was reached at 0.15 U concentration of the enzyme. Therefore, the optimum concentration of enzyme was determined to be 0.15 U. The optimum enzyme immobilization time was examined by changing the immobilization time from 5 to 30 min. It can be seen in Supporting Figure 2B that the maximum current was seen at 15 min of immobilization time. Therefore, the optimum enzyme immobilization time was found to be 15 min. Different concentrations of substrate (5 to 30 µg/mL) were introduced to the enzyme-immobilized PGE/PPy-NPs and the response was monitored. After 15 µg/mL, the signal decreased and then presented a steady line; therefore, this concentration was used [22,24].

3.3.Characterization by SEM

The surface morphologies of pencil graphite electrode (PGE), ZnO, polypyrrole (PPy), Ag-doped ZnO, Ag–XOD, and Ag-doped ZnO–XOD were studied by SEM (Figure 4). PGE (Figure 4A), ZnO (Figure 4B), and PPy (Figure 4C) showed a homogenous surface. Ag-doped ZnO (Figure 4D) showed uniform dispersion, while Ag XOD (Figure 4E) showed unstable dispersion and non-immobilization of XOD. Finally, the Ag-doped ZnO–XOD electrode showed a regular form with electrostatic interaction due to the immobilization of the XOD enzyme (Figure 4F) [6].

3.4.Operational Stability

To define the operational stability of the biosensor, the experiment was carried out 25 times under the optimized biosensor conditions, which are defined in Section 3.2 (0.15 M pyrrole concentration, six scan cycles, 30 mv/s scan rate, 0.15 U enzyme concentration, and 15 µg/mL substrate concentration). As seen from Figure 5A, after 25 experiments, the biosensor retained 76.98% of its initial performance.

3.5.Storage Stability

To define the storage stability of the biosensor, experiments were conducted under the optimized conditions detailed in Section 3.2 (0.15 M pyrrole concentration, six scan cycles, 30 mv/s scan rate, 0.15 U enzyme concentration, and 15 µg/mL substrate concentration). As seen from Figure 5B, after 20 days, the biosensor retained 77.82% of its initial performance.

3.6.Interference Measurements

Interference measurements were conducted using four different interfering substances (hypoxanthine (HX), uric acid (UA), glucose, and ascorbic acid). A 1:1 ratio of these interfering substances was used to determine the effect of interference to the biosensor performance (Figure 5C) [45]. The results showed that, between two additions of 15 µg/mL xanthine, there was no interference between substances on the amperometric response of the biosensor.

3.7.Sensitivity Study

In the current study, we aimed to achieve detection via both amperometry as an electrochemical technique (Supporting Figure 3A) and HPLC (Supporting Figure 3B). Supporting Figure 3A shows the signals, which are provided by different biosensors prepared in the same manner. Relative standard deviation (RSD) values were measured by using the signals in supporting figure 3A. Sensitivity studies were performed to specify the limit of detection (LOD) for both methods. For that reason, the HPLC column and the prepared

biosensor were analyzed using different concentrations of xanthine (linear range between 0.06 and 0.6 μM). Both tested amperometry and HPLC results gave responses between the selected xanthine concentrations. The LOD values were calculated for amperometry and HPLC as 0.07 μM and 0.002 μM, respectively. LOD studies were conducted based on linear regression. For a linear calibration curve, it is assumed that the instrument response y is linearly related to the standard concentration x for a limited range of concentration [46]. This can be expressed in a model such as $y = a + bx$. This model is used to compute the sensitivity b and the LOD. Therefore, the LOD can be expressed as $LOD = 3Sa/b$, where Sa is the standard deviation of the response and b is the slope of the calibration curve [47].

As it can be concluded, the biosensor gave a short response time (3.2 s) with a 0.07 μM LOD (limit of detection), high sensitivity (0.03 μA/mM), and good reproducibility (RSD = 0.54%), while HPLC gave a long response time (30 min) with a 0.002 μM LOD (limit of detection), fair sensitivity (9.06 mA/mM), and good reproducibility (RSD = 0.5%). The biosensor showed operational stability by retaining 76.98% of its initial performance after 25 experiments and it showed storage stability by retaining 77.82% of its initial performance after 20 days. Biosensor-based detection enabled a more sensitive detection of xanthine since HPLC-based detection showed a lower limit of detection. The designed biosensor had a pretty low detection limit compared to the other studies present in the literature, as can be seen in Table 1, and it offers advantages in terms of simplicity and sensitivity.

3.8.Real Fish Meat Sample Experiments by using HPLC and Amperometry

According to the results of the sensitivity study, both methods seem to provide a good LOD that will enable us to perform the detection in real samples. To prove this, sea bass was chosen for the analyses of real samples. The fish samples were bought 0–2 h after the death of the fish and the amount of xanthine determined was noted as the amount at day 0. Fish samples was stored in a refrigerator (4 °C) from day 1 to day 7, until they were spoiled. The fish meat was extracted (using the extraction method described in Section 2.5.1) daily and extraction samples were kept at 4 °C until HPLC (method defined in Section 2.5.2) and amperometry (method defined in Section 2.3.5) analyses were performed. The real fish meat samples (sea bass) were tested by HPLC and amperometry. External standard methods were used to measure the amount of xanthine. Firstly, different concentrations of xanthine (linear range between 0.06 and 0.6 μM) used and the external standard results were compared, these are shown in Supporting Figure 4A for HPLC and Supporting Figure 4B for amperometry. Secondly, the HPLC results of fish meat samples are shown in Figure 6A, while the amperometry results of fish meat samples are shown in Figure 6B. The amperometry studies were examined using the prepared biosensor (0.15 M, pH 7.0; 4 °C; 0.30 mV/s). It can be seen from Figure 6B that there was an increase of the oxidation current observed in the presence of xanthine. However, a sharp oxidation peak was not observed. Therefore, it can be concluded that xanthine detection was conducted successfully with the amperometric technique. From the first storage day to the seventh storage day, the amount of xanthine in fish meat decreased. Thus, xanthine shows in the early stage of fish meat spoilage as a

biomarker. The correlation between the HPLC and amperometry results concerning fish meat samples is shown in Figure 6C. The two methods (HPLC and amperometry) showed good correlation as there were no significant differences between xanthine amounts, which means that the prepared biosensor can be used as an alternative for HPLC (Figure 6C).

4. Conclusion

Due to population increase, limited resources of food, changing lifestyles, and increasing demand for fast food, biosensors are expected to be highly used in the food industry. However, the biosensor technology for the food industry is in its early stages.

The most widely studied biosensors for the food industry are xanthine-based biosensors, which are biomarkers of the early stage of fish meat spoilage. Fish meat is an essential source of protein and other nutrients for humans; however, it is very sensitive and easily spoiled. That is why it is highly important to detect xanthine in fish meat samples.

Traditional technologies (such as HPLC) are labor-intensive, time-consuming, and relatively costly. Herein, a novel biosensor was prepared successfully to detect and determine the xanthine content of fish meat samples. Analysis of fish meat samples was conducted simultaneously and successfully using HPLC and amperometry. It can be concluded that the proposed biosensor is a good and practical alternative to detect the xanthine content of fish meat sample instead of HPLC. The prepared biosensor with its 0.0308 μA/mM sensitivity and high selectivity can easily be applied for other types of meat and meat products and could also be adapted to portable device fabrication.

Author's contribution

B.Y.S. designed and carried out experiments on HPLC and nanomaterials production and characterization, while B.Y.S. and M.K. carried out experiments on biosensor optimization and amperometry studies. B.Y.S. and M.K. prepared manuscript, while E.C., M.O., and S.O. finalized the paper with their scientific perspective.

Funding

This research received no external funding.

The conflict of interest

The authors declare that there is no conflict of interest.

Acknowledgment

B.Y. Sahyar wishes to thank Whirlpool Corporation, specifically Mehmet Acar for his support with doctoral studies. B.Y. Sahyar also wishes to thank Serdar Yildirim for his support on nanomaterials production and characterization.

References

[1] W.W. Westerfield, D.A. Richert, E. S. Higgins, Further studies with xanthine oxidase inhibitors, the journal of biological chemistry 234 (7) (1959) 1897-1900.

[2] W.C. Fraizer, D.C. Westhoff, Contamination, preservation and spoilage of fish and other seafood, Food Microbiology, McGraw Hill Book Company (1978) 244-254.

[3] E. A. Foegeding, T.C. Lanier, H.O. Hultin, Characteristics of edible muscle tissues, Food Chemistry, Fennema, O. R. (Ed.); Marcel Dekker, Inc. 3rd ed. (1996), New York, 879-942.

[4] D. Shan, Y. Wang, H. Xue, S. Cosnier, Sensitive and selective xanthine amperometric sensors based on calcium carbonate nanoparticles, Sens. Actuators B 136 (2009) 510–515.

[5] A.S. Hernández-Cázares, M.C. Aristoy, F. Toldrá, Hypoxanthine-based enzymatic sensor for determination of pork meat freshness, Food Chemistry 123 (2010) 949–954.

[6] R. Devi, M. Thakur, C.S. Pundir, Construction and application of an amperometric xanthine biosensor based on zinc oxide nanoparticles -polypyrrole composite film, Biosensors and Bioelectronics 26 (2011) 3420–3426.

[7] T. Saito, K. Aria, M. Matsuyoshi, A new method for estimating the freshness of fish, Bull. Jpn. Soc. Sci. Fish 24 (1959) 749–750.

[8] L. Mao, F. Xu, Q. Xu, L. Jin, Miniaturized amperometric biosensor based on xanthine oxidase for monitoring hypoxanthine in cell culture media, Anal. Biochem. 292 (2001) 94.

[9] H.S. Nakatani, L.V. Santos, C.P. Pelegrine, S.D.M. Gomes, M. Matsushita, N.E. Souza, J.V. Visentainer, Biosensor based on xanthine oxidase for monitoring hypoxanthine in fish meat, American Journal of Biochemistry and Biotechnology 1 (2005) 85-89.

[10] K. Hegnerová, M. Piliarik, M. Šteinbachová, Z. Flegelová, H. Černohorská, J. Homola, Detection of bisphenol A using a novel surface plasmon resonance biosensor, Anal Bioanal Chem. 398 (2010) 1963–1966.

[11] J. Oracz, E. Nebesny, D. Zyzelewicz, New trends in quantification of acrylamide in food products, Talanta 86 (2011) 23– 34.

[12] C.S. Pundir, R. Devi, J. Narang, S. Singh, J. Nehra, S. Chaudhry, Fabrication of an amperometric xanthine biosensor based on polyvinylchloride membrane, Journal of Food Biochemistry 36 (2012) 21–27.

[13] R.Q. Olojoa, R.H. Xiab, J.J. Abramsona, Spectrophotometric and fluorometric assay of superoxide ion using 4-chloro-7-nitrobenzo-2-ox a-1,3-diazole, Analytical Biochemistry 339 (2005) 338–344.

[14] M. Dervisevic, E. Custiuc, E. Cevik, M. Senel, Construction of novel xanthine biosensor by using polymeric mediator/MWCNT nanocomposite layer for fish freshness detection, Food Chemistry 181 (2015) 277–283.

[15] T. Toyo'oka, T. Kashiwazaki, M. Kato, On-line screening methods for antioxidants scavenging superoxide anion radical and hydrogen peroxide by liquid chromatography with indirect chemiluminescence detection, Talanta 60 (2003) 467-475.

[16] J.S. Beckman, D.A. Parks, J.D. Pearson, P.A. Marshall, B.A. Freeman, A sensitive fluorometric assay for measuring xanthine dehydrogenase and oxidase in tissues, Free Radical Biology and Medicine 6 (6) (1989) 607-615.

[17] Y. Liu, S. Liu, Z. Liu, Screening and determination of potential xanthine oxidase inhibitors from Radix Salviae Miltiorrhizae using ultrafiltration liquid chromatography–mass spektrometry, Journal of Chromatography B 923–924 (2013) 48-53.

[18] D. Yao, A.G. Vlessidis, N.P. Evmiridis, Y. Zhou, S. Xu, H. Zhou, Novel chemiluminescence method for detection of superoxide anions and its application to dry-cured meat, Analytica Chimica Acta 467 (2002) 145–153.

[19] M.J. Vazquez, B. Rodriguez, C. Zapatero, D.G. Tew, Determination of phosphate in nanomolar range by an enzyme-coupling fluorescent method, Analytical Biochemistry 320 (2003) 292–298.

[20] X-X. Wang, Q. Wu, Z. Shan, Q-M. Huang, BSA-stabilized Au clusters as peroxidase mimetics for use in xanthine detection, Biosensors and Bioelectronics 26 (2011) 3614–3619.

[21] A.C. Torres, M.E. Ghica, C.M.A. Brett, Design of a new hypoxanthine biosensor: xanthine oxidase modified carbon film and multi-walled carbon nanotube/carbon film electrodes, Anal Bioanal Chem. 405 (2013) 3813–3822, DOI 10.1007/s00216-012-6631-1.

[22] C. Pundir, R. Devi, Biosensing methods for xanthine determination: A review, Enzyme and Microbial Technology 57 (2014) 55–62.

[23] R. Jain, N. Jadon, A. Pawaiya, Polypyrrole based next generation electrochemical sensors and biosensors: A review, Trends in Analytical Chemistry 97 (2017) 363-373.

[24] H. Xue, S. Mu, Bioelectrochemical response of the polypyrrole xanthine oxidaseelectrode, J Electroanal Chem. 397 (1995) 241–247.

[25] S.N. Lowrence, R.P. Deo, J. Wang, Comparison of the electrochemical reactivity of electrodes modified with carbon nanotubes from different sources, Electroanalysis 17 (2005) 65–72.

[26] Y. Yan, M. Al-Jassim, D.-H. Wei, Doping of ZnO by group-ib elements, Appl. Phys. Lett. 89 (18) (2006) 181912.

[27] D. Sahu, N. Panda, B. Acharya, A. Panda, Enhanced uv absorbance and photoluminescence properties of ultrasound assisted synthesized gold doped ZnO nanorods, Opt. Mater. 36 (8) (2014) 1402–1407.

[28] Y. Ma, G.T. Du, S.R. Yang, Z.T. Li, B.J. Zhao, X.T. Yang, T.P. Yang, Y.T. Zhang, D.L. Liu, Control of conductivity type in undoped ZnO thin films grown by metalorganic vapor phase epitaxy, J. Appl. Phys. 95 (11) (2004) 6268–6272.

[29] O. Lupan, L. Chow, L.K. Ono, B.R. Cuenya, G. Chai, H. Khallaf, S. Park, A. Schulte, Synthesis and characterization of Ag-or Sb-doped ZnO nanorods by a facile hydrothermal route, J. Phys. Chem. C 114 (29) (2010) 12401–12408.

[30] M. Erol, O. Sancakoglu, M. Yurddaskal, S. Yildirim, E. Celik, A Comparison on Physical, Structural, and Photocatalytical Properties of TiO_2 Nanopowders Produced Using Sol-Gel and Flame Spray Pyrolysis, Int. J. Appl. Ceram. Technol. 10(6) (2013) 931–938, DOI:10.1111/ijac.12018.

[31] Y.T. Chung, M.M. Ba-Abbad, A.W. Mohammad, N.H. Hayati Hairoma, A. Benamor, Synthesis of minimal-size ZnO nanoparticles through sol–gel method: Taguchi design optimization, Materials and Design 87 (2015) 780–787.

[32] M. Kaplan, T. Kilic, G. Guler, J. Mandli, A. Amine, M. Ozsoz, A novel method for sensitive microRNA detection: Electropolymerization based doping, Biosensors and Bioelectronics 92 (2017) 770–778.

[33] T. Kilic, A. Erdem, Y. Erac, M. O. Seydibeyoglu, S. Okur, M. Ozsoz, Electrochemical Detection of a Cancer Biomarker mir-21 in Cell Lysates Using Graphene Modified Sensors, Electroanalysis 27 (2015), 317-326.

[34] V. Musat, B. Teixeira, E. Fortunato, R.C.C. Monteiro, P. Vilarinho, Al-doped ZnO thin films by sol–gel method, Surface and Coatings Technology 180 –181 (2004) 659–662.

[35] Z.R. Khan, M.S. Khan, M. Zulfequar, M.S. Khan, Optical and Structural Properties of ZnO Thin Films Fabricated by Sol-Gel Method, Materials Sciences and Applications 2 (2011) 340-345.

[36] Z.B. Bahsi, A.Y. Oral, M.H. Aslan, E. Kayahan, M. Ozer, Sintering Behaviour of ZnO:Cu Ceramics Fabricated by Sol–Gel Derived Powders, ACTA PHYSICA POLONICA A 121 (1) (2012) 271-273.

[37] M. García-Alamo, O. Rodriguez-Nava, A.J. Morales-Ramírez, M. García-Hernández, D. Jaramillo-Vigueras, Synthesis and antibacterial properties of ZnO:Ag films prepared from a Triton containing solution, Materials 6 (2013).

[38] S.A. Ansari, M.M. Khan, J. Lee, M.H. Cho, Highly visible light active Ag@ZnO nanocomposites synthesized by gel-combustion route, Journal of Industrial and Engineering Chemistry 20 (4) (2014), 1602-1607.

[39] O. Bechambi, M. Chalbi, W. Najjar, S. Sayadi, Photocatalytic activity of ZnO doped with Ag on the degradation ofendocrine disrupting under UV irradiation and the investigation of itsantibacterial activity, Applied Surface Science 347 (2015) 414–420.

[40] B.M. Rajbongshi, A. Ramchiary, S.K. Samdarshi, Influence of N-doping on photocatalytic activity of ZnO nanoparticles under visible light irradiation, Materials Letters 134 (2014) 111–114.

[41] S.M. Hosseini, I. Abdolhosseini Sarsari, P. Kameli, H. Salamati, Effect of Ag doping on structural, optical, and photocatalytic properties of ZnO nanoparticles, Journal of Alloys and Compounds 640 (2015) 408–415.

[42] K. Saoud, R. Alsoubaihi, N. Bensalah, T. Bora, M. Bertino, J. Dutta, Synthesis of supported silver nano-spheres on zinc oxide nanorods for visible light photocatalytic applications, Materials Research Bulletin 63 (2015) 134–140.

[43] T.C. Gokoglan, S. Soylemez, M. Kesik, S. Toksabay, L. Toppare, Selenium containing conducting polymer based pyranose oxidase biosensor for glucose detection, Food Chemistry, 172 (2015) 219-224.

[44] D.P. Dubal, S.H. Lee, J G. Kim, W.B. Kim, C.D. Lokhande, Porous polypyrrole clusters prepared by electropolymerization for a high performance supercapacitor, J. Mater. Chem. 22 (2012) 3044.

[45] F. Arslan, A. Yasar, E. Kilic, An Amperometric Biosensor for Xanthine Determination Prepared from Xanthine Oxidase Immobilized in Polypyrrole Film, Artificial Cells, Blood Substitutes, and Biotechnology 34 (2006) 113-128.

[46] Analytical Procedures and Methods Validation: Chemistry, Manufacturing, and Controls, Federal Register (Notices) 65 (2000) 776-777.

[47] A. Shrivastava, V. B. Gupta, Methods for the determination of limit of detection and limit of quantitation of the analytical methods, Chronicles of Young Scientists 2 (1) (2011) 21-25.

[48] U. Jain, J. Narang, N. Chauhan, Enhanced electrochemical performance of xanthine biosensor by core - shell magnetic nanoparticles and carbon nanotube interface, Adv. Mater. Lett. 7(6) (2016) 472-479.

[49] B. Dalkıran, P.E. Erden, E. Kılıç, Construction of an electrochemical xanthine biosensor based on graphene/cobalt oxide nanoparticles/chitosan composite for fish freshness detection, JOTCSA 4 (1) (2017) 23-44.

[50] B. Dalkıran, C. Kaçar, P.E. Erden, E. Kılıç, Electrochemical xanthine biosensor based on zinc oxide nanoparticles–multiwalled carbon nanotubes–1,4-benzoquinone composite, Journal of the Turkish Chemical Society, Section A: Chemistry 5 (1) (2018) 317-332.

FIGURES

Schematic 1. Experimental steps followed throughout the study: (1) the electropolymerization of pyrrole onto pencil graphite electrode (PGE), (2) the entrapment of nano ZnO (A) and nano Ag–ZnO (B) onto PGE doped with polypyrrole, (3) the immobilization of xanthine oxidase (XOD) enzymes, and (4) the electrochemical measurement.

Figure 1. (A); (B) charge transfer resistance (R_{ct}) values of nano ZnO (represented with the black curve), nano Al-doped ZnO (represented with the red curve), nano Ag-doped ZnO (represented with the green curve), nano Cu-doped ZnO (represented with the blue curve) and nano Md-ZnO (represented with the cyan curve) for nano ZnO and nano Ag–ZnO nanoparticles.

Figure 2. Characterization of nano ZnO (represented with the black color) and nano Ag–ZnO (represented with the red color) nanoparticles by (A) X-ray diffraction (XRD); (B) FTIR; and (C) X-ray photoelectron spectrometry (XPS).

Figure 3. Optimization of (A) the pyrrole concentration (curve's represented with the black for 0.01M, red for 0.05M, blue for 0.1M, dark cyan for 0.15M, magenta for 0.2M, and dark yellow for 0.25M), (B) the number of cycles for electropolymerization (curve's represented with the black for 2, red for 4, green for 6, blue for 8, and cyan for 10 number of cycles), (C) the scan rate (curve's represented with the black for 20mV/s, red for 30mV/s, blue for 40mV/s, dark cyan for 50mV/s, magenta for 100mV/s, and dark yellow for 200mV/s).

Figure 4. SEM images of the prepared biosensors: (A) graphite (PGE), (B) ZnO, (C) polypyrrole (PPy), (D) Ag-doped ZnO, (E) Ag–XOD, and (F) Ag-doped ZnO–XOD.

Figure 5. (A) Operational stability and (B) storage stability for biosensor. (C) Interference effect of glucose, uric acid (UA), and ascorbic acid (AA) to the current response of xanthine in 0.05 M, pH 7.4 PBS at +0.70 V.

Figure 6. Xanthine measurements of fish meat samples using (A) HPLC and (B) the prepared biosensor (0.05 M, pH 7.4 PBS at +0.70 V). (C) Correlation between HPLC (represented with the blue color) (Adj. R-Square=0.97, standard error (Intercept)=0.7127 and standard error (Slope)=0.15552) and amperometry methods (represented with the red color) (Adj. R-Square=0.91, standard error (Intercept)=1.22782 and standard error (Slope)=0.026793) regarding the amount of xanthine of fish meat samples.

SUPPORTING FIGURES

Supporting Figure 1. Optimization of (A) the pyrrole concentration, (B) the number of cycles for electropolymerization, (C) the scan rate.

Supporting Figure 2. Optimization of (A) the enzyme concentration, and (B) the time of enzyme immobilization.

Supporting Figure 3. Calibration curves for (A) the amperometric response of the prepared biosensor (Adj. R-Square=0.97, standard error (Intercept)=6.8834E-4 and standard error

(Slope)=0.00185) and (B) the HPLC results (Adj. R-Square=0.99, standard error (Intercept)=0.00184 and standard error (Slope)=0.0129).

Supporting Figure 4. Xanthine as an external standard measurement using (A) HPLC and (B) the prepared biosensor (0.05 M, pH 7.4 PBS at +0.70 V).

Table 1. Analytical performance of the xanthine biosensors reported in literature.

Electrode	Response Time (s)	Sensitivity	Linear Range (μM)	LOD (μM)	Ref
XOD/ZnO-NPs–PPy/Pt electrode	5	-	0.8-40	0.8	[6]
P(GMA-co-VFc)/MWCNT/XO	*4*	16 mA/M	2-48	0.12	[14]
XOD/MNPs/c-MWCNT/FTO	3	-	0.05-150	0.05	[48]
XOD/Co_3O_4 NPs/CH/GR/GCE	10	6.58 μA/mM	0.5-80	0.2	[49]
XOD/BQ-MWCNTs-ZnO-CS/GCE	10	39.4 μA/mMcm^2	$9*10^{-4}$-0.11	0.9	[50]
XOD/nano Ag-ZnO/PPy/PGE	*3.2*	0.0308 μA/mM	0.06-0.6	0.07	Current Work

Highlights

- Conducting polymer polypyrrole on the pencil graphite electrode has been used.
- Ag-doped ZnO nanoparticles increased porous structure and electrode surface area.
- Enzymatic response due to nanoparticle has increased.

Graphical abstract